Hindawi
International Journal of Aerospace Engineering
Volume 2024, Article ID 2582680, 16 pages
https://doi.org/10.1155/2024/2582680

Research Article

A New Theoretical Method for Solving Forward Kinematics of the Parallel Mechanisms Based on Transfer Matrix

Jin Wang,[1,2,3] Zijian Jing,[1,2] Junli Guo,[1,2,3] Tao Qin,[1,2] Han Li,[1,2] Xin Li,[1,2,3] Zhenchuang Li,[1,2,3] Fanhui Meng,[1,2,3] and Bo Qi[1,2,3]

[1]*Key Laboratory of Optical Engineering, Chinese Academy of Sciences, Chengdu 610209, China*
[2]*Institute of Optics and Electronics, Chinese Academy of Sciences, Chengdu 610209, China*
[3]*University of Chinese Academy of Sciences, Beijing 100049, China*

Correspondence should be addressed to Bo Qi; qibo@ioe.ac.cn

Received 20 October 2023; Revised 22 January 2024; Accepted 1 February 2024; Published 26 February 2024

Academic Editor: Jinchao Chen

The flexible parallel mechanism is widely utilized in precision instruments, thanks to its numerous advantages, such as high precision, frictionless operation, and seamless movements. The establishment of the motion equations for this mechanism is crucial for designing, analyzing, controlling, and simulating parallel mechanisms. While the existing inverse kinematics solution theory is comprehensive, developing a forward solution model is challenging due to the nonlinear nature of the attitude equation. To address this issue, a new method based on the transfer matrix approach is proposed in this research to calculate the forward kinematics of parallel mechanisms. The proposed method is applied to analyze the forward kinematics and workspace of both planar and spatial flexible mechanisms. Simulation calculations and experiments are conducted to verify the method's effectiveness. The results demonstrate that the error is approximately 2%, indicating the feasibility and accuracy of the calculation method.

1. Introduction

The flexible parallel mechanism, which uses the flexible deformation of the structure to transmit motion and force, has become a new type of high-sensitive transmission mechanism. Compared with parallel mechanisms using traditional rigid kinematics pairs, the flexible parallel mechanism has the advantages of small size, no friction loss, smooth movement, and no gaps. And it undoubtedly plays a vital role in precision instruments [1–3]. For this reason, a large number of researches and applications on flexible parallel mechanisms have been carried out in recent years. As we all know, the expression of the solution equation is highly nonlinear with respect to the pose variable of the moving platform, generally multiple which leads to solutions. This makes solving the forward kinematics problem of the parallel platform often more complicated than solving the inverse kinematics problem. The forward kinematics solution is the basic theoretical support for controlling the motion of the mechanism and plays an important guiding role in further improving the motion performance of the parallel mechanism points and understanding and analyzing the dynamic behavior of the system. So research on it has always been of top priority.

Huang et al. proposed a method to solve the forward kinematics of the 3-PRS parallel mechanism by combining D-H method and graphic visualization [4]. Wang et al. calculated the positive motion solution of the 3-RUS/RRR platform by designing equivalent spherical joints and adding position sensors to the joints of the constraint chain [5]. Ye et al. used the Sylvester dialysis elimination method and the symmetric elimination method of the 2-UPU/SP PM mechanical structure to obtain the closed solution of the forward kinematics of the 2-UPU/SP-RR five-degree-of-freedom hybrid robot [6]. Masouleh et al. studied the formulation of the forward kinematics problem of 5-RPUR parallel mechanism through the application of the result method and the linear implicit algorithm in the seven-dimensional motion space [7]. Zhang et al. use BP neural

network based on position compensation to effectively solve redundant 2-RPU-2-SPR parallel mechanisms [8]. Mazare et al. used geometric constraints to obtain the positive solution equation of the 3-[P2(US)] mechanism through simplification and elimination [9]. Mingchao et al. proposed to use the current function value to replace the Jacobian matrix that needs to be constructed in the iterative process and to use the quasi-Newton method to solve the forward kinematics of the parallel mechanism [10]. Gallardo-Alvarado solved the forward kinematics problem of the 3-RRS mechanism using the Newton-homotopy continuation method [11]. It can be seen that the methods for solving the forward kinematics solution are mainly numerical, analytical, and neural network and other methods. The characteristic of the numerical method is that the mathematical model is simple to establish, but the amount of calculation is large, the speed of calculation is slow, and the results of calculation may not converge. The characteristic of the analytical method is that the calculation result is not sensitive to the initial value and can obtain all the solutions, but the mathematical derivation process is complicated. Therefore, in view of the above problems, this paper proposes a theoretical method for the forward motion analysis of parallel mechanisms based on the multibody system transfer matrix method (MSTMM). The MSTMM method was originally used to study the dynamics of multibody systems with transfer matrices [12]. In this paper, it is applied to the forward kinematics solution of the parallel mechanism. The modeling is flexible, concise, and operable.

2. Theoretical Modeling Analysis

The parallel mechanism is a closed-loop mechanism with multiple branches in parallel, and its topology diagram is shown in Figure 1. We can clearly understand the internal connection of the parallel mechanism from this figure, providing the basis for establishing the kinematics analysis model below. "m" represents the branch chain number of the mechanism, and "n" represents the component number of each branch chain. $S_{n,m}$ represents the component "n" located in branch "m." And S_{out} represents the terminal output platform of the flexible parallel mechanism.

2.1. Forward Kinematics Analysis. Contrary to the inverse solution of kinematics, the process of solving the forward kinematics solution of a parallel mechanism refers to the process of solving the changes in the position and orientation of the end platform by knowing the length changes of each branch chain of the mechanism or the motion parameters. Therefore, the key to analyzing the forward kinematics solution of the mechanism is how to establish the functional relationship between the changes in the end platform's posture $q = [x, y, z, \theta_x, \theta_y, \theta_z]$ and the changes in the motion parameters of each joint $L = [L_1, L_2, \cdots L_i]$. To realize the control, calibration, and motion planning of the parallel mechanism, it is necessary to solve the forward kinematics problem.

To solve the positive motion solution, it is first necessary to establish the extended state vectors $Z_{n,m}$ and Z_{out}. $Z_{n,m}$ is

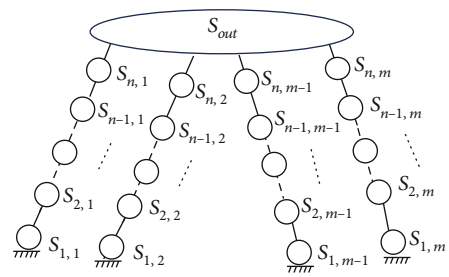

Figure 1: Topological relationship diagram of parallel mechanism.

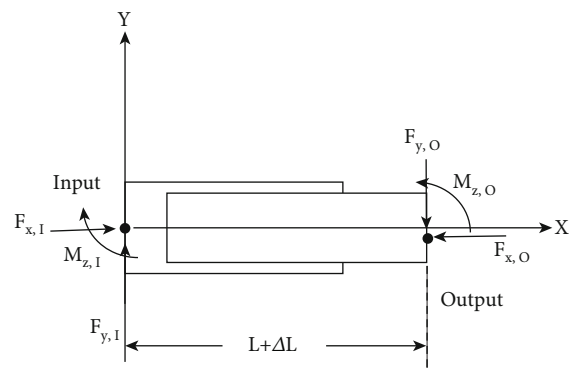

Figure 2: Schematic diagram of the translational joint (in plane).

the state of each unit in each branch chain. Z_{out} is the state vector of the output platform at the end of the mechanism. $Z_{i,n}$ and $Z_{o,n}$ represent the input and output state vectors of unit n, respectively. The state vector includes the displacement and force vector information of the unit and also reflects the change in the branch chain length of the mechanism [13–15].

$$\begin{cases} Z_{o,n} = \left[X, Y, Z, \Theta_x, \Theta_y, \Theta_z, M_x, M_y, M_z, Fx, Fy, Fz, \Delta L_m\right]_n^T, \\ Z_{i,n} = \left[X, Y, Z, \Theta_x, \Theta_y, \Theta_z, M_x, M_y, M_z, Fx, Fy, Fz, \Delta L_m\right]_n^T. \end{cases} \tag{1}$$

Secondly, the transfer matrix/equation of each characteristic unit in the mechanism should be established. For the establishment of common rigid body and flexible unit transfer matrix/equation, please refer to "Transfer matrix method for multibody systems: theory and applications" [12].

It should be noted that, because the transfer matrix is established on the premise of dynamic analysis, when used in the kinematics analysis of parallel mechanisms in this article, the frequency term "ω" is equal to zero or infinitely close to zero. In addition, what needs to be emphasized here is the establishment of the transfer matrix of the moving pair in the parallel mechanism (taking the planar case as an example).

Figure 2 is a schematic diagram of the translational joint with an initial length of L and a variation of ΔL. "I" is the input point, and "O" is the output point. The coordinate system is established with point "I" as the origin of coordinate [16]. From the geometric relationship, the rotation angle of "O" around the Z-axis is the same as that of "I," and the

displacement of "O" can be represented by the displacement of "I" and the angular displacement of "I" around the Z-axis. Considering that the rotation angle around the Z-axis is relatively small, and $|\theta_{Z,I}| << 1$, the relationship can be obtained:

$$\begin{cases} x_O = x_I - by\theta_{Z,I}, \\ y_O = x_I + bx\theta_{Z,I}, \\ \theta_{Z,O} = \theta_{Z,I}. \end{cases} \tag{2}$$

According to the force balance formula,

$$\begin{cases} F_{O,x} = F_{I,x}, \\ F_{O,y} = F_{I,y}, \\ M_{Z,O} = M_{Z,I} - byF_{I,x} + bxF_{I,x}, \end{cases} \tag{3}$$

where (bx, by) is the coordinate of output point "O" relative to point "I" and $bx = L + \Delta L$. Further, the above formula is written in matrix form:

$$Z_O = UZ_I. \tag{4}$$

Here, the transfer matrix of the translational joint can be divided into two parts: $U = U_1 + U_2$. U_1 is the basic transfer matrix including the excitation force "F," which is consistent with the transfer matrix of common rigid body elements:

$$U_1 = \begin{bmatrix} 1 & 0 & 0 & 0 & 0 & 0 & 0 \\ 0 & 1 & L & 0 & 0 & 0 & 0 \\ & 0 & 1 & 0 & 0 & 0 & 0 \\ 0 & 0 & 0 & 1 & 0 & L & f_{41} \\ 0 & 0 & 0 & 0 & 1 & 0 & f_x \\ 0 & 0 & 0 & 0 & 0 & 1 & f_y \\ 0 & 0 & 0 & 0 & 0 & 0 & 1 \end{bmatrix}, \tag{5}$$

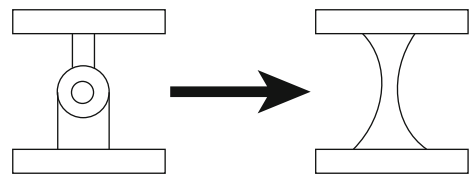

Figure 3: Pseudo-flexible body model.

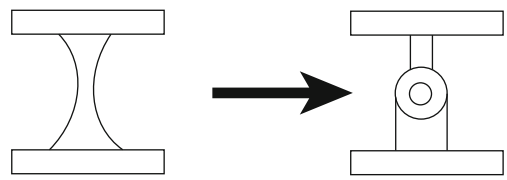

Figure 4: Pseudorigid body model.

where $f_{41} = m_z + f_x(y - b_y) - f_y(b_x - x)$. f_x and f_y are the components of the translational joint under the action of the simple excitation force $F = [f_x, f_y]^T$ and moment m_z at point (x, y).

U_2 is the displacement transfer matrix including the variation ΔL of the translational joint:

$$U_2 = \begin{bmatrix} \text{zeros}(1,2) & \text{zeros}(1,1) & \text{zeros}(1,2) & \text{zeros}(1,1) & A \\ \text{zeros}(1,2) & \Delta L_m & \text{zeros}(1,2) & \text{zeros}(1,1) & \text{zeros}(1,1) \\ \text{zeros}(1,2) & \text{zeros}(1,1) & \text{zeros}(1,2) & \text{zeros}(1,1) & \text{zeros}(1,1) \\ \text{zeros}(1,2) & \text{zeros}(1,1) & \text{zeros}(1,2) & \Delta L_m & \text{zeros}(1,1) \\ \text{zeros}(3,2) & \text{zeros}(3,1) & \text{zeros}(3,2) & \text{zeros}(3,1) & \text{zeros}(3,1) \end{bmatrix}. \tag{6}$$

It should be noted here that when the driving mode is displacement, $A = 1$; when the driving mode is force, both A and ΔL are 0. The establishment of the transfer matrix/equation for the moving pair in a spatial state is similar to that of a planar matrix, which also includes the same basic transfer matrix U_1 as traditional rigid body elements, as well as the displacement transfer matrix U_2 with displacement increments.

$$U_2 = \begin{bmatrix} \text{zeros}(1,4) & \text{zeros}(1,4) & \text{zeros}(1,4) & \text{zeros}(1,4) & \text{zeros}(1,4) & \text{zeros}(1,4) & A \\ \text{zeros}(1,4) & \text{zeros}(1,4) & \Delta L_m & \text{zeros}(1,4) & \text{zeros}(1,4) & \text{zeros}(1,4) & \text{zeros}(1,4) \\ \text{zeros}(1,4) & \Delta L_m & \text{zeros}(1,4) & \text{zeros}(1,4) & \text{zeros}(1,4) & \text{zeros}(1,4) & \text{zeros}(1,4) \\ \text{zeros}(4,4) & \text{zeros}(1,4) & \text{zeros}(1,4) & \text{zeros}(4,4) & \text{zeros}(1,4) & \text{zeros}(1,4) & \text{zeros}(1,4) \\ \text{zeros}(1,4) & \text{zeros}(1,4) & \text{zeros}(1,4) & \text{zeros}(1,4) & \text{zeros}(1,4) & \Delta L_i & \text{zeros}(1,4) \\ \text{zeros}(1,4) & \text{zeros}(1,4) & \text{zeros}(1,4) & \text{zeros}(1,4) & \Delta L_m & \text{zeros}(1,4) & \text{zeros}(1,4) \\ \text{zeros}(4,4) & \text{zeros}(4,4) & \text{zeros}(4,4) & \text{zeros}(4,4) & \text{zeros}(4,4) & \text{zeros}(4,4) & \text{zeros}(4,4) \end{bmatrix}. \tag{7}$$

Input: The change value of the mobile pair in each branch chain
Output: The state vector of the mechanism-driven platform

```
Set A=1, ω=0.0001; F=0
for Min ≤ΔL_1 ≤ Max (start length to to end length)
  for Min ≤ΔL_2 ≤ Max (start length to to end length)
    for Min ≤ΔL_m ≤ Max (start length to to end length)
      Build a mathematical model of the organization ((1)–(18))
      if θ_Main ≤ hinge angle ≤θ_max
        Output the state vector of the moving platform to the aggregate
      end
    end
  end
end
Plot the state vectors satisfying the condition in space
```

Algorithm 1: Calculate the orientation workspace of the flexible four-bar mechanism.

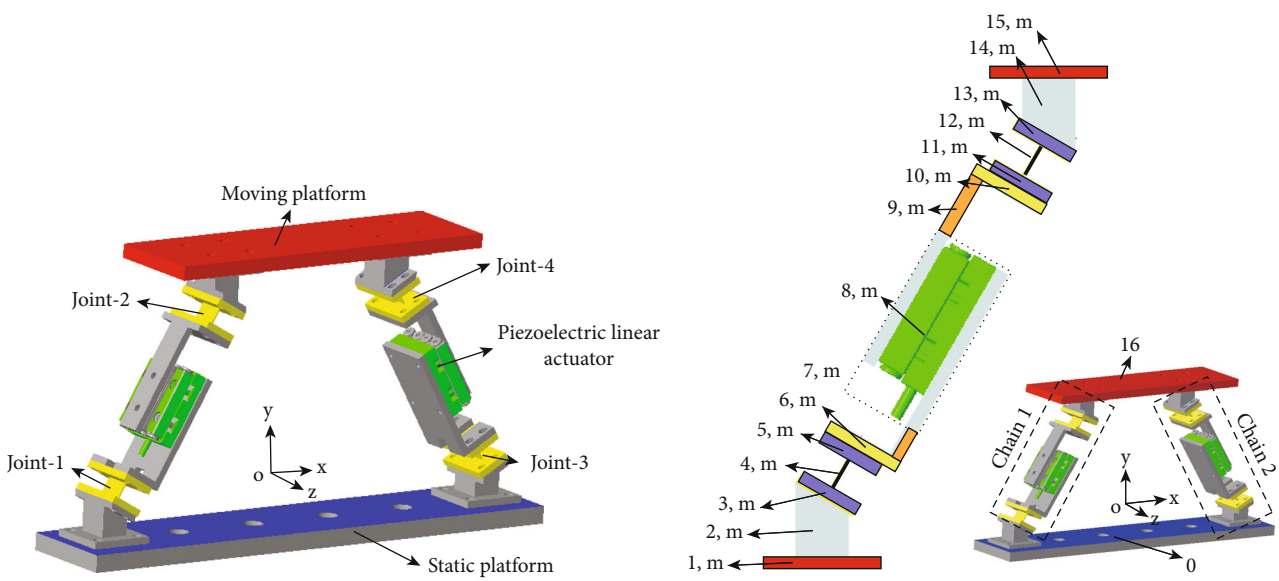

(a) 3D diagram of mechanism

(b) Schematic diagram of branch chain and unit

Figure 5: Flexible four-bar mechanism.

According to the relationship between each unit, a transfer equation is used to establish the connection between the branch chain neutron unit and the branch chain, and finally, the branch chain transfer matrix is spliced into a unified parallel mechanism transfer matrix/equation. The state vector at the end of each branch chain can be obtained by multiplying each subunit together.

$$Z_{\text{out},m} = U_{n,m} \cdots U_{2,m} U_{1,m} Z_{\text{start},m}. \tag{8}$$

$Z_{\text{start},m}$ represents the state vector of the starting unit in branch chain m, that is, $Z_{1,m}$. $Z_{\text{out},m}$ represents the output state vector of the end unit in branch chain m. $U_{n,m}$ represents the transfer matrix of unit n in branch chain m.

The state vector at the end of the final moving platform is as follows:

$$Z_{\text{out}} = U_{\text{out}}(E_1 Z_{\text{out},1} + E_2 Z_{\text{out},2} + \cdots + E_m Z_{\text{out},m}), \tag{9}$$

$$E_{\text{out},1} Z_{\text{out},1} = E_{\text{out},2} Z_{\text{out},2}, \tag{10}$$

$$E_{\text{out},1} Z_{\text{out},1} = E_{\text{out},m} Z_{\text{out},m}, \tag{11}$$

where

$$E1 = \begin{bmatrix} \text{eye}(13) \\ \text{zeros}(7(m-1), 13) \end{bmatrix}, \tag{12}$$

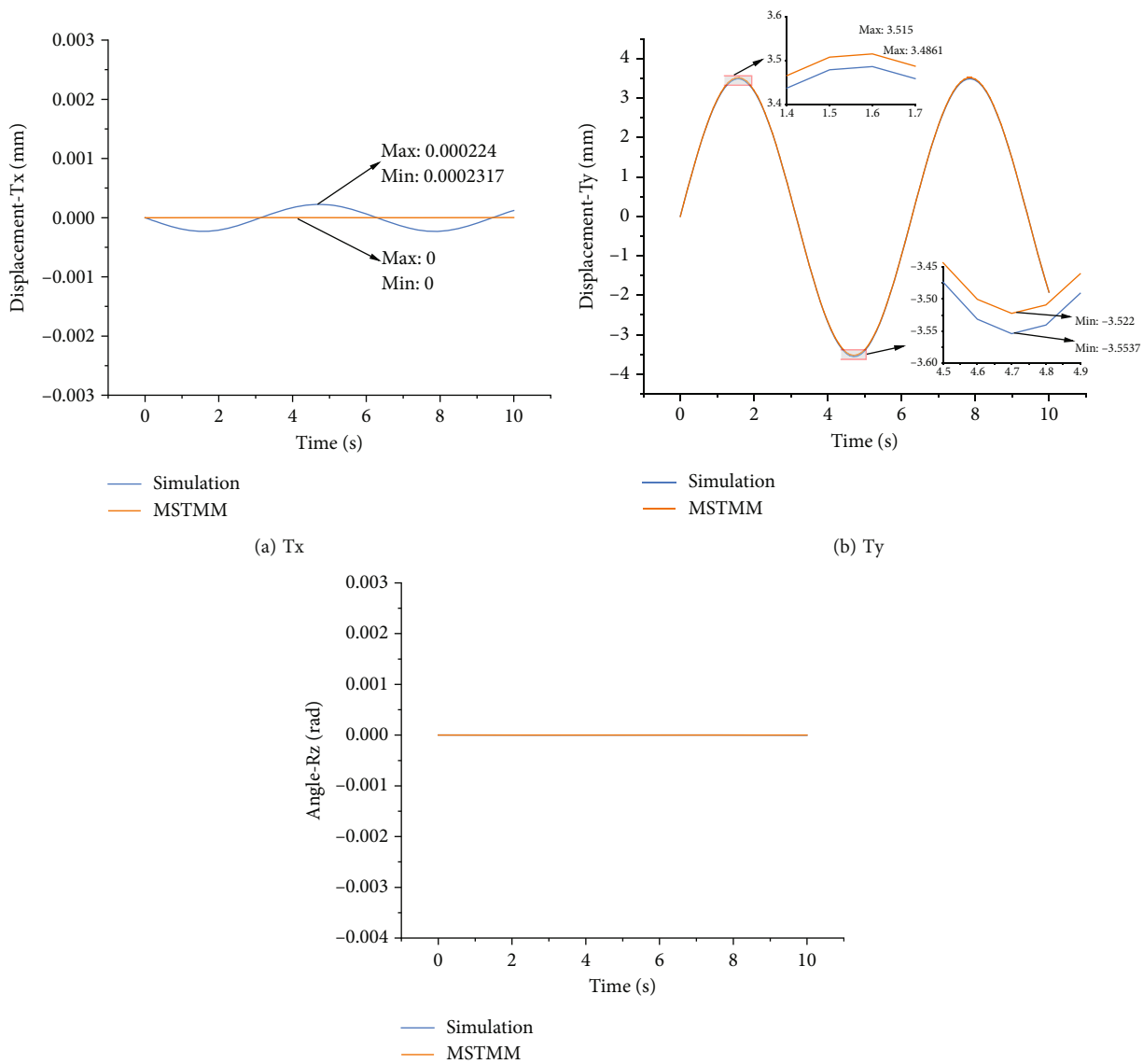

Figure 6: Output result of the moving platform with the change of translational joints: $3*\sin(t)$.

$$E2 = \begin{bmatrix} \text{zeros}(13,6) & \text{zeros}(13,7) \\ \text{zeros}(7,6) & \text{eye}(7) \\ \text{zeros}(7(m-2),6) & \text{zeros}(7(m-2),7) \end{bmatrix}, \quad (13)$$

$$Em-k = \begin{bmatrix} \text{zeros}(13,6) & \text{zeros}(13,7) \\ \text{zeros}(7(m-k-2),6) & \text{zeros}(7(m-k-2),7) \\ \text{zeros}(7,6) & \text{eye}(7) \\ \text{zeros}(7k,6) & \text{zeros}(7k,7) \end{bmatrix}, \quad (14)$$

$$Em = \begin{bmatrix} \text{zeros}(13+7(m-2)) & \text{zeros}(13+7(m-2),7) \\ \text{zeros}(7,6) & \text{eye}(7) \end{bmatrix}, \quad (15)$$

where $k < m$,

$$E_{\text{out},1} = [\text{eye}(6) \quad \text{zeros}(6,7)], \quad (16)$$

$$E_{\text{out},m} = \begin{bmatrix} \text{eye}(3) & -Li,\text{out\_}m & \text{zeros}(3,7) \\ \text{zeros}(3,3) & eye(3) & \text{zeros}(3,7) \end{bmatrix}, \quad (17)$$

$$Li,\text{out}_m = \begin{bmatrix} 0 & -a_3 & a_2 \\ a_3 & 0 & -a_1 \\ -a_2 & a_1 & 0 \end{bmatrix}, \quad (18)$$

where (a_1, a_2, a_3) is the coordinates of the output point of branch chain m relative to the input point of branch chain 1. "zeros(a, b)" represents a matrix of zeros in row a and column b. "eye(a)" represents the $a \times a$ identity matrix.

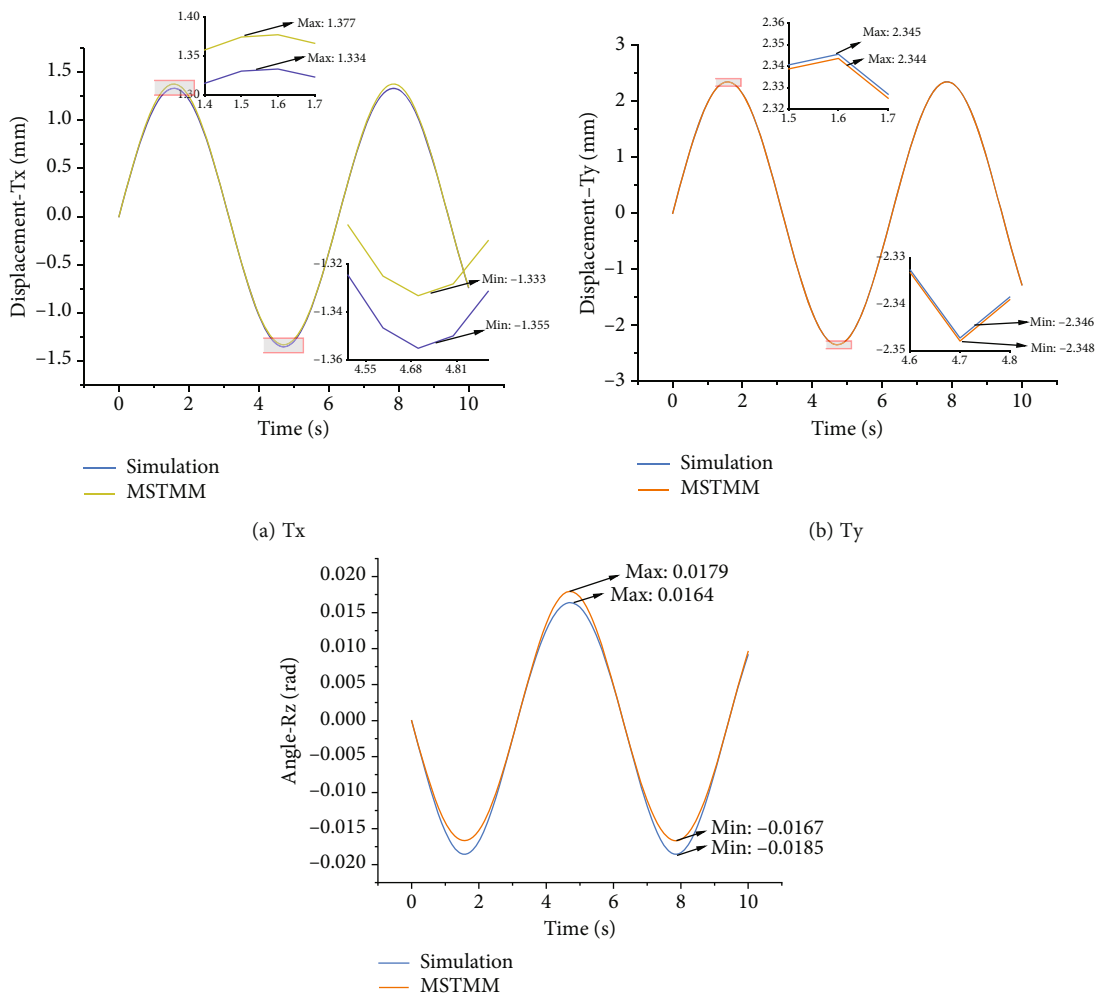

Figure 7: Output result of the moving platform with the change of translational joint 1: $3*\sin(t)$ and translational joint 2: $\sin(t)$.

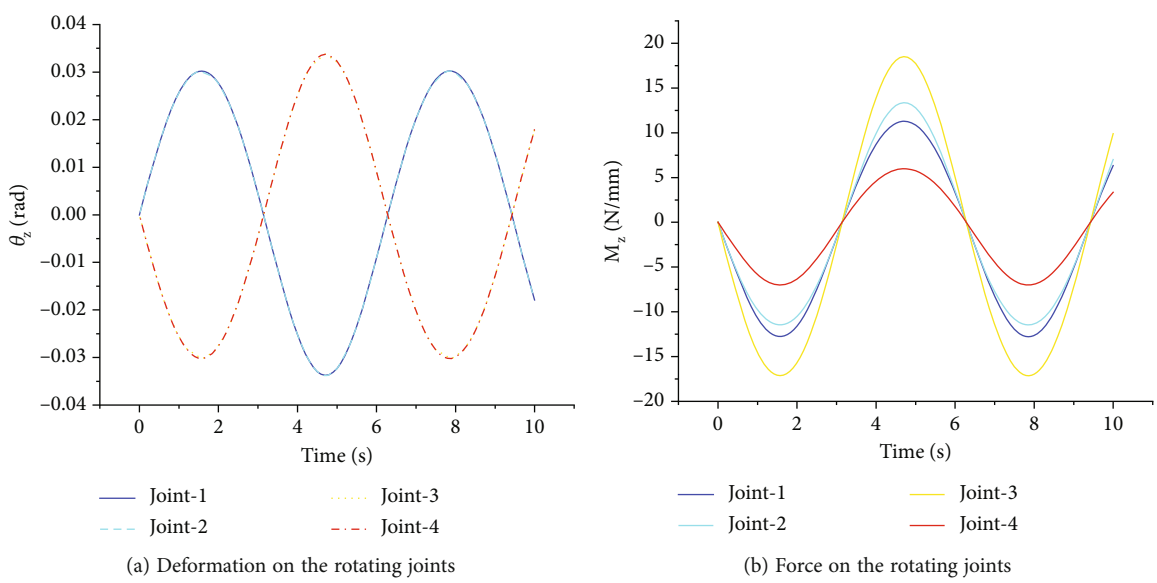

Figure 8: Rotation joint deformation and force curve.

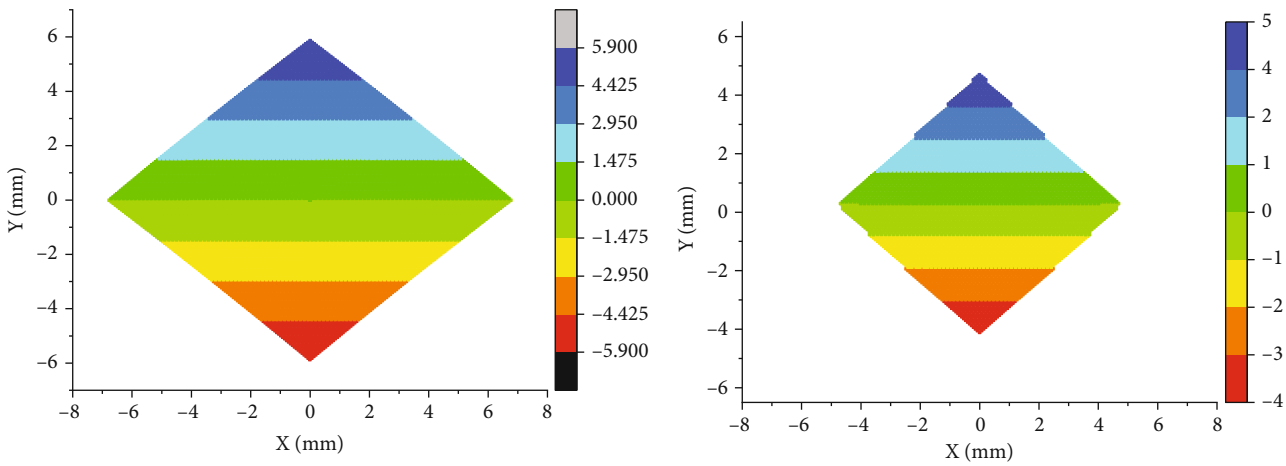

(a) Limit of the moving pair variation

(b) Limit of the moving pair variation and hinge deformation

Figure 9: Working place of the flexible four-bar mechanism.

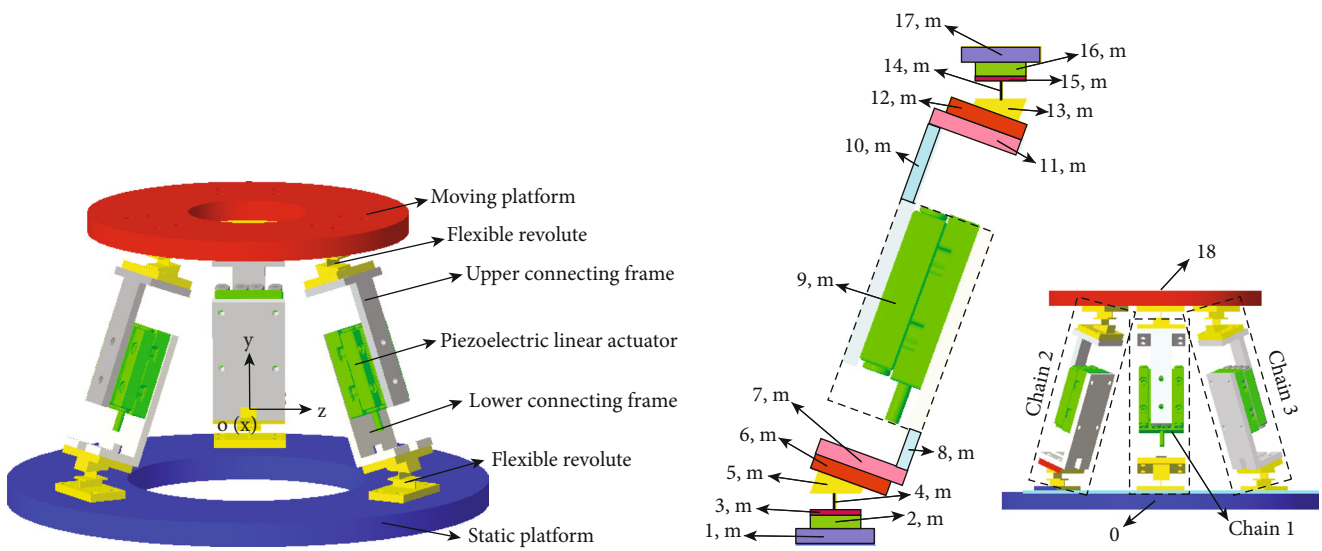

(a) 3D diagram of mechanism

(b) Schematic diagram of branch chain and unit

Figure 10: 3-UPU mechanism.

Finally, the results are postprocessed for the total transfer equation. Through this method, we can conduct a simple and efficient analysis of parallel mechanisms, with good operability and easy programming.

For the rigid parallel mechanism, we can equivalently replace the rigid kinematics pair with a flexible hinge to establish a "pseudoflexible model" (see Figure 3) and further use this method to perform forward kinematics calculations according to the actual situation. The pseudorigid body model (see Figure 4) uses rigid mechanism theory to analyze the compliant mechanism, whereas the pseudoflexible model is just the opposite [17].

2.2. Position Inverse Solution. The inverse kinematics of the parallel mechanism is to solve the changes of each joint through the pose of the end platform, and its calculation method is very well developed. The most common method for solving the motion inverse solution of the mechanism is to use the rod length formula and coordinate changes. Regarding this aspect, this article will no longer analyze [18–21].

2.3. Workspace. The working range to which the end of the moving platform of the parallel mechanism can run is the working space of the parallel mechanism. Because it is affected by the length of the rod, the deformation range of the hinge, and the internal interference, the analysis of the working space is also an important consideration in reflecting the mechanism's execution ability [22]. Due to the complexity of solving the forward solution of motion, methods such as the three-dimensional (3D) boundary/polar

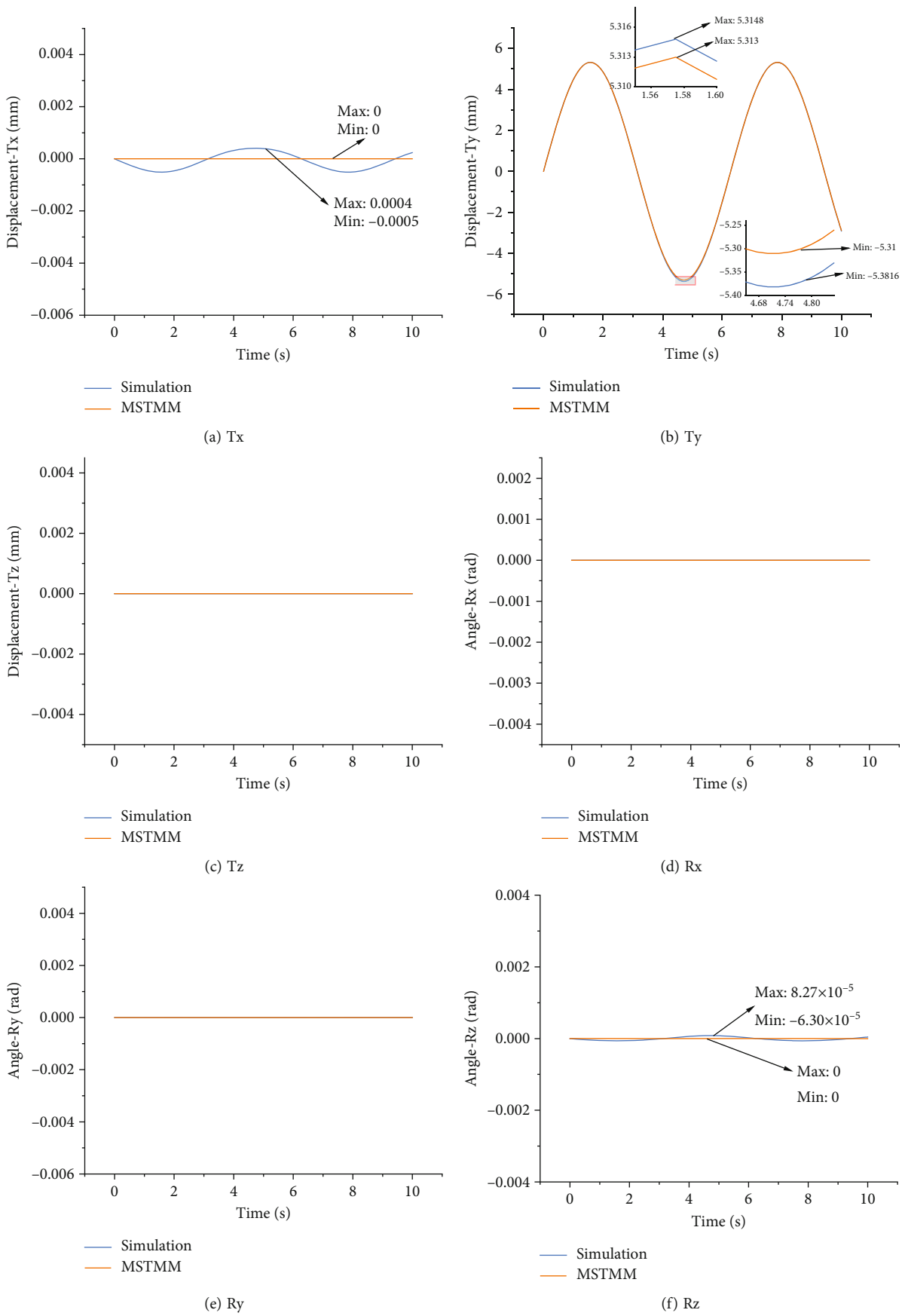

Figure 11: Output result (6-Dof) of the moving platform with the change of translational joints: $5*\sin(t)$.

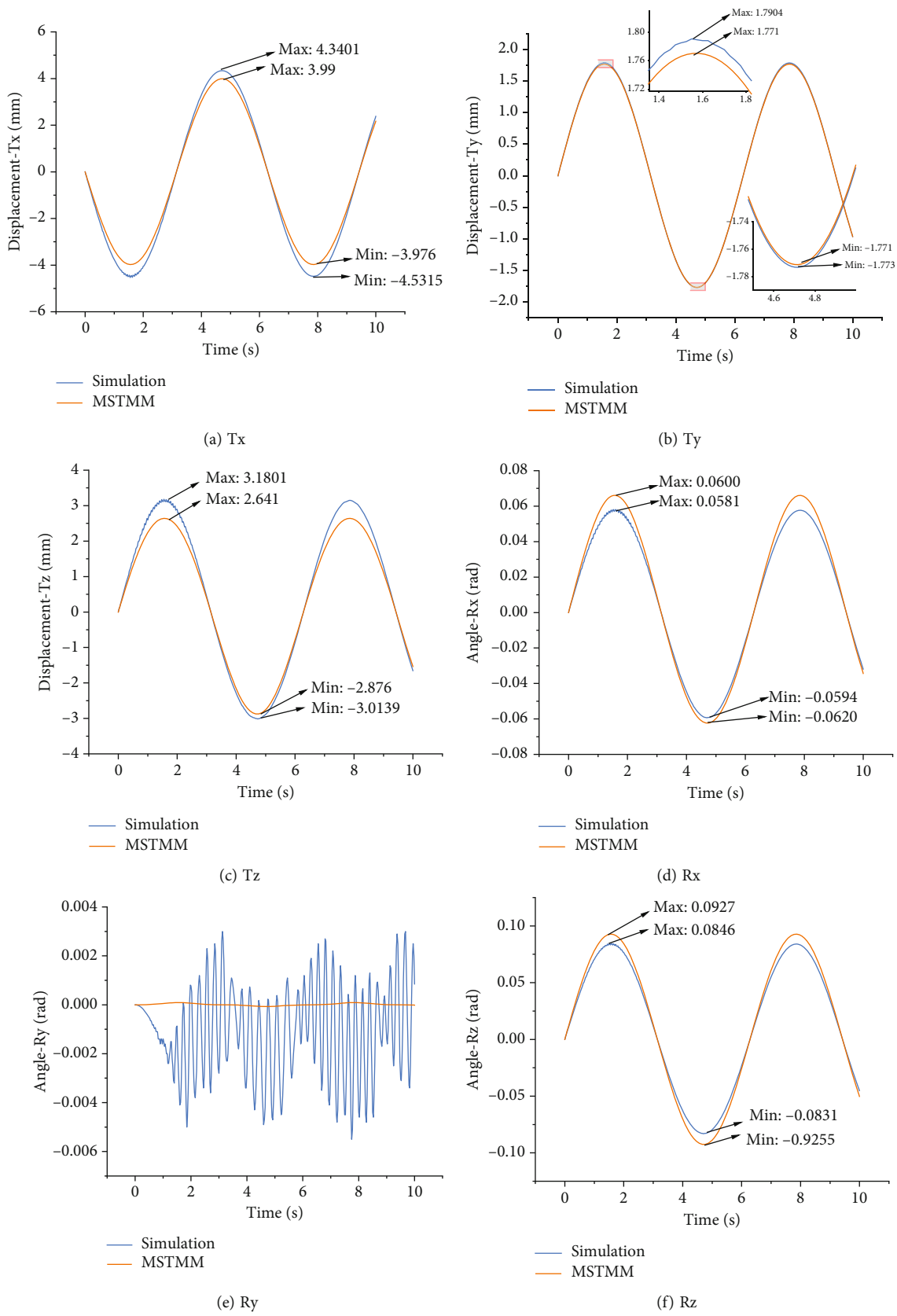

Figure 12: Output result (6-Dof) of the moving platform with the change of translational joint 1: 5∗sin(t), translational joint 2: -2∗sin(t), and translational joint 3: 2∗sin(t).

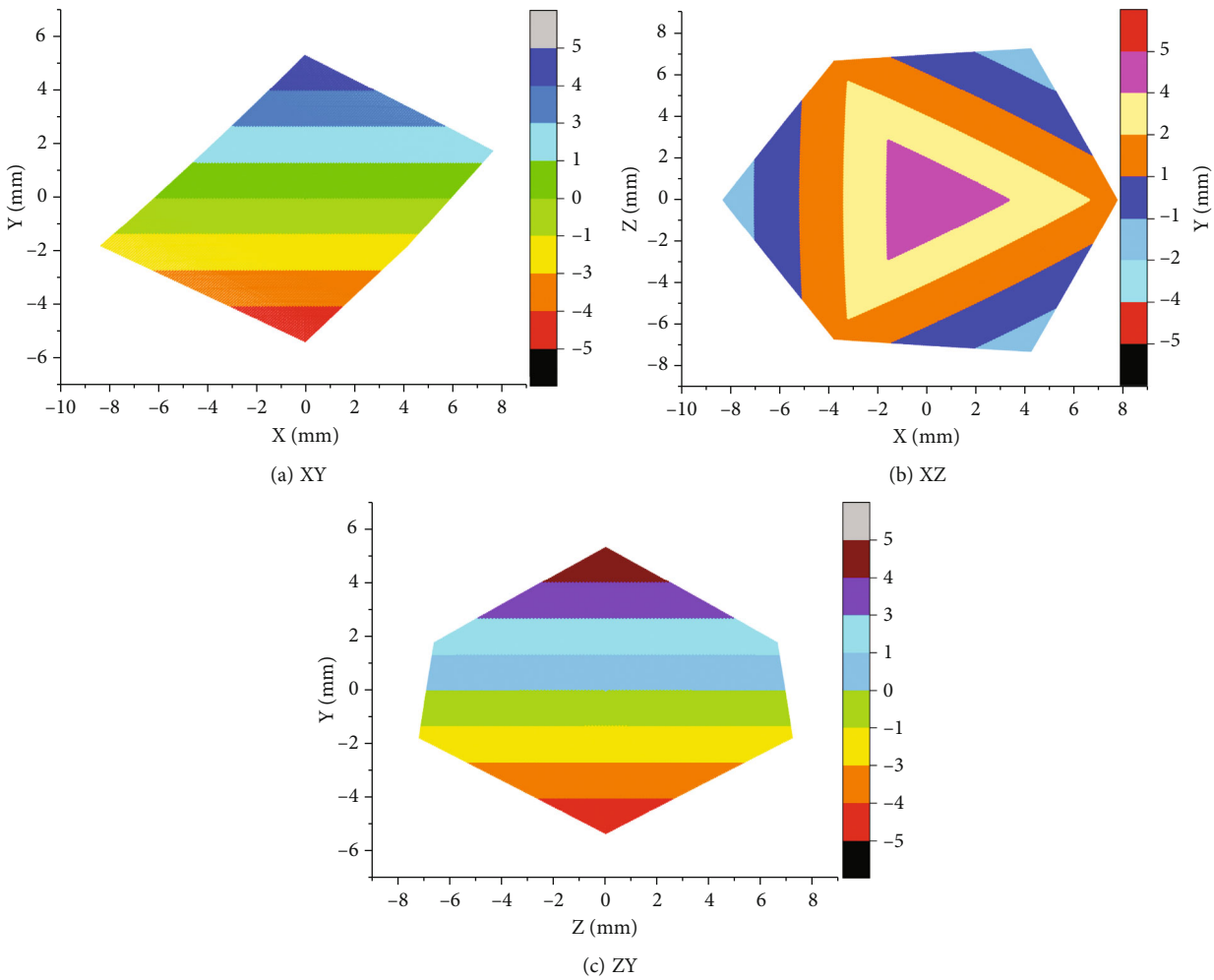

Figure 13: Working space of 3-UPU mechanism.

coordinate search method [23–25], which were used previously, are based on the condition of the inverse solution equation and Monte Carlo method [26, 27]. Based on the above forward kinematics solution, this paper uses the forward numerical calculation method to obtain the state vector of each hinge and the position coordinates of the corresponding end platform by limiting the elongation range of the translational joint of each branch chain. Finally, output the position coordinates of all end-moving platforms that meet the specified conditions, in order to obtain the working space of the mechanism (See Algorithm 1).

Table 1: Specific parameters of SLC-1720 actuator.

Parameter	Value
Dimensions(mm × mm × mm)	22 × 17 × 8.5
Max. lift force F (N)	>1.5
Trval (mm)	±6
Scan resolution (nm)	<1
Step width (nm)	1-150
Max. frequency (kHz)	18.5

3. Planar Mechanism—Flexible Four-Bar Mechanism

3.1. Forward Kinematics. As we all know, the parallel mechanism with definite motion should satisfy the condition that the number of degrees of freedom is less than or equal to the number of driving. However, the specific number of degrees of freedom of the underconstrained mechanism is actually greater than the number of branches and the number of driving. This causes the Jacobian matrix of the mechanism to be a non-full-rank matrix, which affects the stability of the mechanism. When the length of the rod remains constant, there are multiple solutions for the position, and a rigid four-bar linkage serves as such a structure [28, 29].

In order to consider changing the matrix from a nonfull rank to a full rank, under the condition that the displacement constraint has been added, we need to restrict it through other constraints, such as force constraints. Therefore, the unique elastic deformation properties of flexible materials

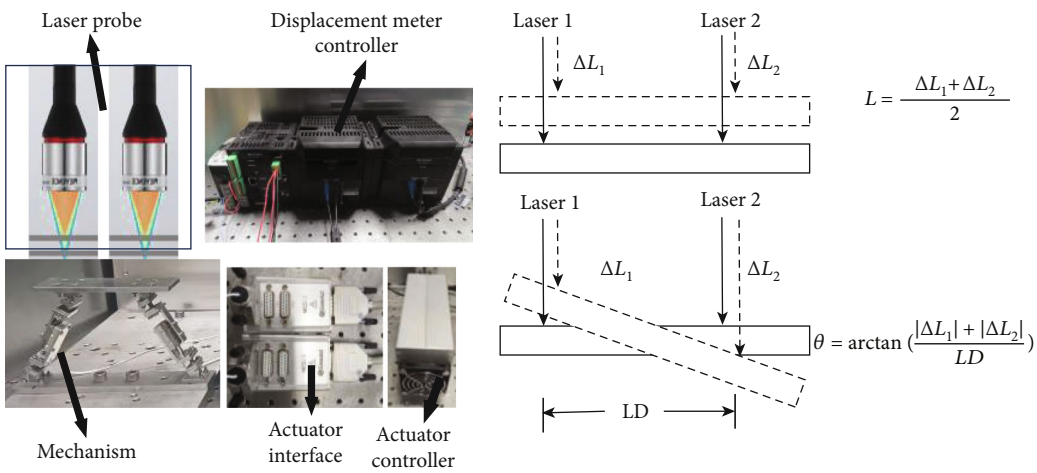

(a) Experimental measurement device

(b) Experimental measurement principle

Figure 14: Diagram of experimental measurement device.

can be exploited to increase force constraints. By replacing the rigid kinematics pair in the uncertain mechanism with the flexible hinge, the Jacobian matrix of the mechanism is satisfied with full rank, the unique solution of the mechanism motion is realized, and the problem of uncontrollability of the uncertain kinematics mechanism is solved.

The kinematics and other related analyses of the flexible four-bar mechanism will be carried out below. Figure 5 is a 3D diagram of the flexible four-bar mechanism and a schematic diagram of each branch unit.

From the above formulas ((1)–(18)), the transfer matrix/equation (plane) can be derived ((A.5)–(A.7) in Appendix A):

$$U_{\text{all}} Z_{\text{all}} = 0,$$

$$U_{\text{all}} = \begin{bmatrix} U_{16}E_1U_{15.1}U_{14.1}\cdots U_{2.1}U_{1.1} & U_{16}E_2U_{15.2}U_{14.2}\cdots U_{2.2}U_{1.2} & -\text{eye}(7) \\ E_{\text{out},1}U_{15.1}U_{14.1}\cdots U_{2.1}U_{1.1} & -E_{\text{out},2}U_{15.2}U_{14.2}\cdots U_{2.2}U_{1.2} & \text{zeros}(3,7) \end{bmatrix} Z_{\text{all}} = \begin{bmatrix} Z_{\text{start},1} \\ Z_{\text{start},2} \\ Z_{\text{out}} \end{bmatrix}. \tag{19}$$

By substituting various parameter values and solving the equation, the state vector at the end of the parallel platform can be obtained, with the following result:

Figures 6 and 7 show that the curve trends of the simulation and calculation results of the flexible four-bar mechanism under two input conditions are consistent. Figure 6 shows that the translation error of the moving platform in the main direction Y between the two results is 0.9%. The error in the X direction is 0.3%, and the rotational error in the Z direction is negligible. Figure 7 shows that the errors in the X, Y, and Z directions between the two results are within 3%, 0.1%, and 10%, respectively. The main reasons for the discrepancy between the two are as follows: (1) there is an error in the processing of the flexible unit in the kinematics simulation software and (2) the stress concentration area is not taken into account in the calculation model.

According to the calculation model, we can also understand the rotation and force of each hinge simply and quickly, as shown in Figure 8. This method facilitates our modeling process and provides great convenience to understand the inner operating mechanism of the parallel mechanism.

3.2. Workspace. According to the above description of the mechanism's working range algorithm, Figure 9 shows the working range of the mechanism before and after considering constraints. The focus here is to illustrate the feasibility of this mathematical model for solving the mechanism workspace, so the constraints are directly assumed to be as follows:

(1) The moving pair variation range is ±5

(2) The hinge deformation range is ±2pi/180 rad (In the actual calculation process, the calculation should be carried out according to the maximum deformation formula of the hinge)

Results are obtained according to the algorithm in Section 2.2. It can be clearly seen that the working range in Figure 9(b) is significantly smaller than the range in Figure 9(a) without considering the hinge, indicating that the working range of the hinge also directly affects the working range of the output platform at the end of the mechanism.

Table 2: Translational principal direction measurement.

Translational joint		MSTMM	Experiment								
			First			Second			Third		
1	2		Point 1	Point 2	Error	Point 1	Point 2	Error	Point 1	Point 2	Error
μm	μm	rad	μm	μm	—	μm	μm	—	μm	μm	—
0	0	0	0	0	—	0	0	—	0	0	—
1	1	1172.3	1161.8	1160.9	-0.93%	1161.1	1160.4	-0.99%	1161.4	1160.4	-0.97%
2	2	2343.9	2310.9	2327	-1.06%	2321.9	2325.5	-0.86%	2316.3	2326	-0.97%
3	3	3515	3458.6	3473.3	-1.40%	3468.8	3470.1	-1.30%	3462.1	3470.8	-1.38%
4	4	4685.4	4599.1	4618.4	-1.64%	4608.2	4615.4	-1.57%	4600.3	4616.7	-1.64%
5	5	5855.3	5730.6	5760.5	-1.87%	5744.9	5755.9	-1.79%	5736.4	5756.9	-1.86%
4	4	4685.4	4596.5	4619	-1.66%	4605.2	4618.2	-1.57%	4596.7	4619.2	-1.65%
3	3	3515	3456	3472.3	-1.45%	3463.9	3472.9	-1.33%	3456.7	3473.6	-1.42%
2	2	2343.9	2308.9	2326.7	-1.11%	2316	2327.5	-0.95%	2328.3	2328.3	-0.67%
1	1	1172.3	1159.2	1160.9	-1.04%	1163.2	1163.5	-0.76%	1164.5	1164.5	-0.67%
0	0	0	-1.2	-0.6	—	2.3	0	—	-5.1	0.5	—
-1	-1	-1173	-1161.7	-1175.6	-0.37%	-1167.6	-1170.7	-0.33%	-1172	-1173.5	-0.02%
-2	-2	-2346.6	-2343.9	-2354	0.10%	-2333.7	-2350.9	-0.18%	-2339.6	-2352.2	-0.03%
-3	-3	-3521.1	-3522	-3541.3	0.30%	-3517	-3538.7	0.19%	-3523.6	-3540	0.30%
-4	-4	-4696.3	-4716.1	-4738.6	0.66%	-4701.7	-4736.5	0.49%	-4712.5	-4736.8	0.60%
-5	-5	-5872.4	-5915.1	-5948.5	1.01%	-5910.3	-5945.4	0.94%	-5918.5	-5945.6	1.02%
-4	-4	-4696.3	-4706.5	-4740.4	0.58%	-4701.7	-4739.1	0.51%	-4710.2	-4738.8	0.60%
-3	-3	-3521.1	-3519.2	-3543.3	0.29%	-3512.3	-3542.5	0.18%	-3521.6	-3542.3	0.31%
-2	-2	-2346.6	-2340.6	-2356.3	0.08%	-2326.8	-2355.7	-0.23%	-2336	-2355.2	-0.04%
-1	-1	-1173	-1159.6	-1175.9	-0.45%	-1158.9	-1176.8	-0.44%	-1168.4	-1175.8	-0.08%
0	0	0	0.8	-0.8	—	12.5	-1.5	—	2	-0.5	—

4. Space Mechanism—3-UPU Mechanism

After the analysis of the planar mechanism in the previous chapter, we can clearly find the feasibility and accuracy of calculating the parallel mechanism based on the improved transfer matrix method. In this chapter, we will analyze again through the space mechanism to further prove the generality of the method proposed in this paper [30–32].

4.1. Forward Kinematics. The 3-UPU structure, as a typical platform with a full-rank matrix of mechanisms, has a definite trajectory and was taken here as an example. According to the analysis steps of this calculation method, 3-UPU is divided and numbered according to the branch chain it belongs to, as shown in Figure 10.

According to the formulas (1)–(18), the total transfer matrix/equation of the 3-UPU mechanism can be obtained ((B.5)–(B.8) in Appendix B):

$$U_{\text{all}} Z_{\text{all}} = 0$$

$$U_{\text{all}} = \begin{bmatrix} U_{18}E_1U_{17,1}U_{16,1}\cdots U_{2,1}U_{1,1} & U_{18}E_2U_{17,2}U_{16,2}\cdots U_{2,2}U_{1,2} & U_{18}E_3U_{17,3}U_{16,3}\cdots U_{2,3}U_{1,3} & -eye(13) \\ -E_{\text{out},1}U_{17,1}U_{16,1}\cdots U_{2,1}U_{1,1} & E_{\text{out},2}U_{17,2}U_{16,2}\cdots U_{2,2}U_{1,2} & \text{zeros}(6,13) & \text{zeros}(6,13) \\ -E_{\text{out},1}U_{17,1}U_{16,1}\cdots U_{2,1}U_{1,1} & \text{zeros}(6,13) & E_{\text{out},3}U_{17,3}U_{16,3}\cdots U_{2,3}U_{1,3} & \text{zeros}(6,13) \end{bmatrix},$$

$$Z_{\text{all}} = \begin{bmatrix} Z_{\text{start},1} \\ Z_{\text{start},2} \\ Z_{\text{start},3} \\ Z_{\text{out}} \end{bmatrix}. \tag{20}$$

Table 3: Rotational principal direction measurement.

Translational joint		MSTMM	Experiment								
			First			Second			Third		
1	2		Point 1	Point 2	Error	Point 1	Point 2	Error	Point 1	Point 2	Error
μm	μm	rad	μm	μm	—	μm	μm	—	μm	μm	—
0	0	0	0	0	—	0	0	—	0	0	—
1	-1	0.0173	680.9	-511.3	1.33%	678.1	-512	1.15%	677.6	-512	1.11%
2	-2	0.0346	1402.6	-991.5	1.71%	1395.7	-990.7	1.39%	1396.2	-991	1.42%
3	-3	0.0519	2130.9	-1436.5	0.99%	2124.5	-1435.1	0.77%	2124	-1435.1	0.76%
4	-4	0.0694	2900.2	-1853.2	0.56%	2892.8	-1851.1	0.36%	2892	-1850.6	0.33%
5	-5	0.0869	3702.3	-2246.2	0.41%	3694.8	-2244.1	0.25%	3694.3	-2244.4	0.24%
4	-4	0.0694	2887.7	-1844.5	0.11%	2880.7	-1842.4	-0.08%	2880.7	-1842.4	-0.08%
3	-3	0.0519	2109.4	-1425.5	0.07%	2102.7	-1423.1	-0.19%	2103.5	-1423.6	-0.15%
2	-2	0.0346	1371.9	-976.7	-0.22%	1366	-974.9	-0.55%	1366	-974.9	-0.55%
1	-1	0.0173	662.3	-499.5	-1.25%	655.8	-497.9	-1.94%	656.3	-498.2	-1.87%
0	0	0	-12	2.5	—	19.2	5.1	—	-19	4.9	—
-1	1	-0.0173	-660.2	547	2.61%	-664.9	547.6	3.06%	-663.1	546.8	2.84%
-2	2	-0.0346	-1273.4	1111	1.30%	-1279.8	1112.8	1.65%	-1280	1112.8	1.66%
-3	3	-0.0519	-1862.9	1704.7	1.00%	-1870.6	1707	1.28%	-1869.9	1706.7	1.25%
-4	4	0.0694	-2279.7	2337	-2.32%	-2436.4	2345.2	1.16%	-2436.1	2344.7	1.14%
-5	5	-0.0869	-2963	3010.8	0.83%	-2972.7	3015.2	1.07%	-2972.5	3014.9	1.06%
-4	4	0.0694	-2417.2	2334.7	0.53%	-2424.9	2337.5	0.75%	-2425.9	2338	0.78%
-3	3	-0.0519	-1850.6	1703.6	0.62%	-1858.4	1706.2	0.91%	-1858.4	1705.7	0.90%
-2	2	-0.0346	-1257.5	1095.4	-0.04%	-1264.9	1098	0.39%	-1266	1098.5	0.46%
-1	1	-0.0173	-637.7	532.4	-0.55%	-645.2	534.8	0.30%	-645.2	534.8	0.30%
0	0	0	8.9	-2.9	—	1.2	-0.5	—	1.5	-0.8	—

By substituting various parameter values and solving the equation, the state vector at the end of the parallel platform can be obtained. The results are shown in Figures 11 and 12.

It can be seen from Figures 11 and 12 that this method is still feasible for the forward kinematics analysis of space-flexible parallel mechanisms. In the case of different rod lengths, the curve trends of the simulation and calculation results are still consistent. Figure 11 shows that the error between the two results of the mechanism under translation is at the micron level, and the error is within 1%. Figure 12 shows that the translational errors in the X, Y, and Z directions between the two results are around 8.7%, 1.1%, and 17%, respectively, and the rotational errors are around 0.3%, 10%, and 8%, respectively. The reasons for the error between the two are the same as above: (1) there is a processing error of the flexible unit in the kinematics simulation software and (2) the stress concentration area is not considered in the calculation model.

4.2. Workspace. According to the algorithm in Section 2.2, the working range of the 3-UPU mechanism can still be solved simply and quickly (regardless of the mechanism pose). Figure 13 only shows the working range under the constraint of considering the change of the translational joint.

5. Verification Experiment

In this paper, the flexible four-bar mechanism is taken as an example to carry out experiments. The mechanism material is 7075-T6 aluminum alloy, with an elastic modulus of 71.7 GPa, a density of 2.81 kg/m^3, a tensile yield strength of 503 MPa, and a Poisson's ratio of 0.33. This mechanism uses the SLC-1720 product of SmarAct (German) to drive the RPR branch chain, and the specific parameters are shown in Table 1.

In the experimental research, two laser displacement sensors (CL-P070, from Keyence Company) are used to measure the output displacement and angle of the platform, and the specific experimental device is shown in Figure 14.

The results of the experimental tests recorded the main movement direction of the mechanism (see Tables 2 and 3). It can be seen from the table that the test results are highly consistent with the calculation results, and the error between the two is maintained at 1%, which fully proves the feasibility and accuracy of the method. The main causes of errors include mechanism processing and assembly errors, as well as calculation errors caused by stress concentration.

6. Conclusion

In this paper, a mathematical method that can be used to solve the forward kinematics of flexible parallel mechanisms

is proposed. This method can solve all parallel mechanisms' forward kinematics and working space range. In addition, it can also easily calculate the deformation and stress of each component in the mechanism, guiding practical applications.

(1) Taking the flexible planar four-bar mechanism and the spatial 3-UPU mechanism as examples, the feasibility and accuracy of this method for flexible mechanism analysis are verified through kinematics forward solution analysis and solution of the working space range

(2) A "pseudoflexible model" is proposed. The specific measure is to replace the rigid joints in the rigid parallel mechanism with flexible hinges to establish an equivalent pseudoflexible model of the rigid mechanism. Neglecting the maximum deformation of the hinge, the method in this paper can be used to analyze the forward motion of a rigid parallel mechanism

(3) The addition of flexible hinges not only brings movement displacement constraints to the mechanism but also adds force constraints to the mechanism. There is no longer a simple geometric relationship between the elements in the Jacobian matrix of the mechanism, but also force balance conditions. Therefore, flexible hinges can be used to add force constraints to ensure the full rank of the Jacobian matrix of the rigid uncertain mechanism, thereby achieving the purpose of stabilizing and determining the motion of the rigid uncertain mechanism

The establishment of the forward kinematics mathematical model of the parallel mechanism provides a reference for control in actual engineering. In future work, we will focus on dynamic characteristic analysis to establish a unified mathematical model of parallel mechanisms.

Appendix

A. Modeling of flexible four-bar mechanism

The establishment process of the total transfer matrix equation of the flexible four-bar mechanism is as follows:

State vector output from the end of branch 1:

$$Z_{\text{out},1} = U_{15,1}U_{14,1}U_{13,1}U_{12,1}U_{11,1}U_{10,1}U_{9,1}U_{8,1}U_{7,1} U_{6,1}U_{5,1}U_{4,1}U_{3,1}U_{2,1}U_{1,1}Z_{\text{start},1}. \tag{A.1}$$

State vector output from the end of branch 2:

$$Z_{\text{out},2} = U_{15,2}U_{14,2}U_{13,2}U_{12,2}U_{11,2}U_{10,2}U_{9,2}U_{8,2}U_{7,2} U_{6,2}U_{5,2}U_{4,2}U_{3,2}U_{2,2}U_{1,2}Z_{\text{start},2}. \tag{A.2}$$

State vector at the end of the mechanism:

$$\begin{gathered} Z_{\text{out}} = U_{16}E_1Z_{\text{out},1} + U_{16}E_2Z_{\text{out},2}, \\ E_{\text{out},1}Z_{\text{out},1} = -E_{\text{out},2}Z_{\text{out},2}. \end{gathered} \tag{A.3}$$

Integrating the above formulas is as follows:

$$U_{\text{all}}Z_{\text{all}} = 0, \tag{A.4}$$

$$U_{\text{all}} = \begin{bmatrix} U_{16}E_1U_{15,1}U_{14,1}\cdots U_{2,1}U_{1,1} & U_{16}E_2U_{15,2}U_{14,2}\cdots U_{2,2}U_{1,2} & -\text{eye}(7) \\ E_{\text{out},1}U_{15,1}U_{14,1}\cdots U_{2,1}U_{1,1} & -E_{\text{out},2}U_{15,2}U_{14,2}\cdots U_{2,2}U_{1,2} & \text{zeros}(3,7) \end{bmatrix}, \tag{A.5}$$

$$Z_{\text{all}} = \begin{bmatrix} Z_{\text{start},1} \\ Z_{\text{start},2} \\ Z_{\text{out}} \end{bmatrix}. \tag{A.6}$$

Enter boundary conditions:

$$\begin{gathered} Z_{\text{start},1} = \left[0, 0, 0, F_x, F_y, M_z, L_1\right]_{\text{start}}^T, \\ Z_{\text{start},2} = \left[0, 0, 0, F_x, F_y, M_z, L_1\right]_{\text{start}}^T, \\ Z_{\text{out}} = \left[X, Y, \Theta_z, 0, 0, 0, L_1 + L_2\right]^T. \end{gathered} \tag{A.7}$$

Organize the above data and solve equation (A.4) to get the result.

B. Modeling of 3-UPU mechanism

The establishment process of the total transfer matrix equation of the flexible four-bar mechanism is as follows:

State vector output from the end of branch 1:

$$Z_{\text{out},1} = U_{15,1}U_{14,1}U_{13,1}U_{12,1}U_{11,1}U_{10,1}U_{9,1}U_{8,1}U_{7,1}U_{6,1}U_{5,1} U_{4,1}U_{3,1}U_{2,1}U_{1,1}Z_{\text{start},1} \tag{B.1}$$

State vector output from the end of branch 2:

$$Z_{\text{out},2} = U_{15,2}U_{14,2}U_{13,2}U_{12,2}U_{11,2}U_{10,2}U_{9,2}U_{8,2}U_{7,2} U_{6,2}U_{5,2}U_{4,2}U_{3,2}U_{2,2}U_{1,2}Z_{\text{start},2} \tag{B.2}$$

State vector output from the end of branch 3:

$$Z_{\text{out},3} = U_{15,3}U_{14,3}U_{13,3}U_{12,3}U_{11,3}U_{10,3}U_{9,3}U_{8,3}U_{7,3} U_{6,3}U_{5,3}U_{4,3}U_{3,3}U_{2,3}U_{1,3}Z_{\text{start},3} \tag{B.3}$$

State vector at the end of the mechanism:

$$\begin{aligned} Z_{\text{out}} &= U_{18}E_1Z_{\text{out},1} + U_{18}E_2Z_{\text{out},2} + U_{18}E_3Z_{\text{out},3}, \\ E_{\text{out},1}Z_{\text{out},1} &= -E_{\text{out},2}Z_{\text{out},2}, \\ E_{\text{out},1}Z_{\text{out},1} &= -E_{\text{out},3}Z_{\text{out},3}. \end{aligned} \tag{B.4}$$

Integrating the above formulas is as follows:

$$U_{\text{all}}Z_{\text{all}} = 0, \tag{B.5}$$

$$U_{\text{all}} = \begin{bmatrix} U_{18}E_1U_{17,1}\cdots U_{2,1}U_{1,1} & U_{18}E_2U_{17,2}\cdots U_{2,2}U_{1,2} & U_{18}E_3U_{17,3}\cdots U_{2,3}U_{1,3} & -\text{eye}(13) \\ -E_{\text{out},1}U_{17,1}\cdots U_{2,1}U_{1,1} & E_{\text{out},2}U_{17,2}\cdots U_{2,2}U_{1,2} & \text{zeros}(6,13) & \text{zeros}(6,13) \\ -E_{\text{out},1}U_{17,1}\cdots U_{2,1}U_{1,1} & zeros(6,13) & E_{\text{out},3}U_{17,3}\cdots U_{2,3}U_{1,3} & \text{zeros}(6,13) \end{bmatrix}, \tag{B.6}$$

$$Z_{\text{all}} = \begin{bmatrix} Z_{\text{start},1} \\ Z_{\text{start},2} \\ Z_{\text{start},3} \\ Z_{\text{out}} \end{bmatrix}. \tag{B.7}$$

Enter boundary conditions:

$$\begin{aligned} Z_{\text{start},1} &= \left[0, 0, 0, F_x, F_y, M_z, L_1\right]_{\text{start}}^T, \\ Z_{\text{start},2} &= \left[0, 0, 0, F_x, F_y, M_z, L_1\right]_{\text{start}}^T, \\ Z_{\text{start},3} &= \left[0, 0, 0, F_x, F_y, M_z, L_1\right]_{\text{start}}^T, \\ Z_{\text{out}} &= \left[X, Y, \Theta_z, 0, 0, 0, L_1 + L_2 + L_3\right]^T. \end{aligned} \tag{B.8}$$

Organize the above data and solve equation (B.5) to get the result.

Data Availability

All relevant data are within the paper.

Additional Points

Highlights. (i) A new method for solving forward kinematics of parallel mechanisms is proposed. (ii) The pseudoflexible model is proposed in this article. (iii) The mechanism's Jacobian matrix becomes fully rank by increasing force constraints.

Conflicts of Interest

The authors declare that they have no conflicts of interest.

Acknowledgments

This research was funded by the Young Scientists Fund of the National Natural Science Foundation of China (grant number 12003039).

References

[1] C. Gosselin and L.-T. Schreiber, "Redundancy in parallel mechanisms: a review," *Applied Mechanics Reviews*, vol. 70, no. 1, article 010802, 2018.

[2] M. Luces, J. K. Mills, and B. Benhabib, "A review of redundant parallel kinematic mechanisms," *Journal of Intelligent & Robotic Systems*, vol. 86, no. 2, pp. 175–198, 2017.

[3] M. Ling, L. L. Howell, J. Cao, and G. Chen, "Kinetostatic and dynamic modeling of flexure-based compliant mechanisms: a survey," *Applied Mechanics Reviews*, vol. 72, no. 3, article 030802, 2020.

[4] J. Huang, B. Hu, and J. Song, "A solving method for forward kinematics of 3-prs parallel mechanism," *Journal of Mechanical Transmission*, vol. 43, no. 8, pp. 98–102, 2019.

[5] C. Wang, Y. Fang, S. Guo, and Y. Chen, "Design and kinematical performance analysis of a 3-RUS/RRR redundantly actuated parallel mechanism for ankle rehabilitation," *Journal of Mechanisms and Robotics*, vol. 5, no. 4, article 041003, 2013.

[6] H. Ye, D. Wang, J. Wu, Y. Yue, and Y. Zhou, "Forward and inverse kinematics of a 5-dof hybrid robot for composite material machining," *Robotics and Computer-Integrated Manufacturing*, vol. 65, article 101961, 2020.

[7] M. T. Masouleh, C. Gosselin, M. Husty, and D. R. Walter, "Forward kinematic problem of 5-rpur parallel mechanisms

(3t2r) with identical limb structures," *Mechanism and Machine Theory*, vol. 46, no. 7, pp. 945–959, 2011.

[8] H. Zhang, H. Fang, D. Zhang, X. Luo, and Q. Zou, "Forward kinematics and workspace determination of a novel redundantly actuated parallel manipulator," *International Journal of Aerospace Engineering*, vol. 2019, Article ID 4769174, 14 pages, 2019.

[9] M. Mazare, M. Taghizadeh, and M. Rasool Najafi, "Kinematic analysis and design of a 3-dof translational parallel robot," *International Journal of Automation and Computing*, vol. 14, no. 4, pp. 432–441, 2017.

[10] G. Mingchao, Z. Tieshi, W. Chang, C. Yuhang, and H. Yong, "Direct position analysis of parallel mechanism based on quasi-Newton method," *Journal of Mechanical Engineering*, vol. 51, no. 9, pp. 28–36, 2015.

[11] J. Gallardo-Alvarado, "An application of the newton-homotopy continuation method for solving the forward kinematic problem of the 3-rrs parallel manipulator," *Mathematical Problems in Engineering*, vol. 2019, Article ID 3123808, 6 pages, 2019.

[12] X. Rui, G. Wang, and J. Zhang, *Transfer Matrix Method for Multibody Systems: Theory and Applications*, John Wiley & Sons, 2017.

[13] J. Li, X. Zhu, C. Shen, X. Peng, and S. A. Cummer, "Transfer matrix method for the analysis of space-time-modulated media and systems," *Physical Review B*, vol. 100, no. 14, article 144311, 2019.

[14] A. Obradović, S. Šalinić, D. R. Trifković, N. Zorić, and Z. Stokić, "Free vibration of structures composed of rigid bodies and elastic beam segments," *Journal of Sound and Vibration*, vol. 347, pp. 126–138, 2015.

[15] J. Wang, Z. Jing, Z. Xie, Z. Ning, and B. Qi, "Analysis and optimization of dynamic and static characteristics of the compliant-amplifying mechanisms," *Micromachines*, vol. 14, no. 8, p. 1502, 2023.

[16] J. Hu, T. Wen, and J. He, "Dynamics of compliant mechanisms using transfer matrix method," *International Journal of Precision Engineering and Manufacturing*, vol. 21, no. 11, pp. 2173–2189, 2020.

[17] L. L. Howell, "Compliant mechanisms," in *21st Century Kinematics: The 2012 NSF Workshop*, pp. 189–216, Springer, 2013.

[18] X. Liang, X. Zeng, G. Li, T. Su, and G. He, "Kinematic analysis of three redundant parallel mechanisms for fracture reduction surgery," *Mechanism and Machine Theory*, vol. 188, article 105400, 2023.

[19] X. Zhang, H. Wang, Y. Rong et al., "Improved inverse kinematics and dynamics model research of general parallel mechanisms," *Journal of Mechanical Science and Technology*, vol. 37, no. 2, pp. 943–954, 2023.

[20] H. Shen, Z. Du, D. Chablat, J. Li, and G. Wu, "A new 3-dof 2t1r parallel mechanism: topology design and kinematics," 2023, https://arxiv.org/abs/2306.12845.

[21] Z. Zheng, Y. Zhang, Y. Wu, and Y. Li, "3-prrr parallel mechanism kinematics and workspace analysis," in *Journal of Physics: Conference Series, Vol. 2450*, IOP Publishing, 2023.

[22] J. Huang and Y. Li, "Analysis of a novel 2-dof flexure hinge-based parallel micromanipulator in a polar coordinate system," in *2010 IEEE International Conference on Automation and Logistics*, pp. 323–328, Hong Kong, China, 2010.

[23] C. Yonggang, Z. Yuru, and M. Yunzhong, "Workspace analysis and parameter optimization of 6-rss parallel mechanism," *Journal of Mechanical Engineering*, vol. 44, no. 1, pp. 19–24, 2008.

[24] G. Zong-he, D. Jian-guo, H. Xiu-qing, and S. Lei, "Analysis on position and workspace of 4-ptt parallel mechanism," *Transactions of the Chinese Society for Agricultural Machinery*, vol. 39, no. 7, pp. 144–148, 2008.

[25] J. Lei, Y. Cao, and F. Wang, "Workspace analysis of a 4 ups-upu parallel mechanism based on the boundary search method," *Ji Xie She Ji Yu Yan Jiu(Machine Design and Research)*, vol. 29, no. 1, pp. 5–9, 2013.

[26] B. Li, H. Sun, Q. Jia, and G. Chen, "Calculation of space robot workspace by using Monte Carlo method," *Spacecraft Engineering*, vol. 20, no. 4, pp. 79–85, 2011.

[27] Z. Liu, H. Liu, Z. Luo, and X. Zhang, "Improvement on Monte Carlo method for robot workspace determination," *Nongye Jixie Xuebao(Transactions of the Chinese Society of Agricultural Machinery)*, vol. 44, no. 1, pp. 230–235, 2013.

[28] B. Burak, A. Elmas, and O. Ibrahim, "Design and kinematics analysis of a parallel mechanism to be utilized as a luggage door by an analogy to a four–bar mechanism," *Engineering*, vol. 3, no. 4, 2011.

[29] M. Sitti, "Piezoelectrically actuated four-bar mechanism with two flexible links for micromechanical flying insect thorax," *IEEE/ASME Transactions on Mechatronics*, vol. 8, no. 1, pp. 26–36, 2003.

[30] M. B. Dehkordi, A. Frisoli, E. Sotgiu, and M. Bergamasco, "Modelling and experimental evaluation of a static balancing technique for a new horizontally mounted 3-upu parallel mechanism," *International Journal of Advanced Robotic Systems*, vol. 9, no. 5, p. 193, 2012.

[31] D. R. Walter, M. L. Husty, and M. Pfurner, "A complete kinematic analysis of the snu 3-upu parallel robot," *Contemporary Mathematics*, vol. 496, p. 331, 2009.

[32] C. Zhao, Z. Chen, Y. Li, and Z. Huang, "Motion characteristics analysis of a novel 2r1t 3-upu parallel mechanism," *Journal of Mechanical Design*, vol. 142, no. 1, article 012302, 2020.